

Article

Separation and Calibration Method of Structural Parameters of 6R Tandem Robotic Arm Based on Binocular Vision

Rui Wang^{1,2} , Xiangyu Guo³, Songmo Li¹ and Lin Wang^{1,2,*}¹ School of Ocean Engineering, Harbin Institute of Technology at Weihai, Weihai 264209, China² Weihai Key Laboratory of Intelligent Operation and Maintenance, Harbin Institute of Technology, Weihai 264200, China³ School of Mechatronics Engineering, Harbin Institute of Technology, Harbin 150001, China

* Correspondence: wanglin_007@hitwh.edu.cn

Abstract: In this paper, a kinematic separation calibration method of 6R series manipulator is proposed, and its absolute accuracy is improved by a binocular camera and standard sphere. First, a geometric error mapping model for the robotic arm was established, and the error parameters were divided into position parameters and attitude parameters for calibration purposes. Second, in the process of solving error parameters using numerical algorithms, it is easy to encounter matrix ill-conditioned problems. The spectral correction iteration method is introduced to improve the calculation accuracy. Third, three standard balls are installed at the end of the robotic arm as markers, and the center coordinates are measured using a binocular camera to obtain the actual end pose parameters. To verify the effectiveness of the proposed method, a simulation model verification was designed, and the results showed that the separation calibration method was the best. Finally, the IRB-1200 robot was successfully calibrated using the proposed method; the average robot position and angle error after calibration was significantly decreased. The position accuracy was improved by 66.9%, and the attitude accuracy was improved by 86.2%.

Keywords: error calibration; binocular vision; robotic arm; geometric error; ill-conditioned optimization**MSC:** 53A17; 65D19; 65F10; 70B15

Citation: Wang, R.; Guo, X.; Li, S.; Wang, L. Separation and Calibration Method of Structural Parameters of 6R Tandem Robotic Arm Based on Binocular Vision. *Mathematics* **2023**, *11*, 2491. <https://doi.org/10.3390/math11112491>

Academic Editor: António Lopes

Received: 24 March 2023

Revised: 16 May 2023

Accepted: 24 May 2023

Published: 29 May 2023



Copyright: © 2023 by the authors. Licensee MDPI, Basel, Switzerland. This article is an open access article distributed under the terms and conditions of the Creative Commons Attribution (CC BY) license (<https://creativecommons.org/licenses/by/4.0/>).

1. Introduction

A series robotic arm is an open loop motion chain composed of multiple links, with a wide range of motion, multiple functions, and a wide range of applications. As the production scenarios in which tandem robotic arms participate become more complex, offline programming methods are increasingly used in industry. This approach requires a high level of absolute accuracy of the tandem robotic arm to ensure that the tandem robotic arm will accurately reproduce the programmed end effector (EE) pose [1]. However, the absolute accuracy of the current tandem robotic arm is poor (only 2~3 mm). Among the many factors that affect the absolute motion accuracy of the tandem robotic arm, the geometric error, that is, the EE pose error caused by the kinematic parameter error, accounts for about 80% of total errors. Geometric error refers to the deviation between the actual kinematic parameters and theoretical kinematic parameters of the tandem robotic arm caused by the errors in the manufacturing and assembly process of the parts of the tandem robotic arm, movement under continuous high load, collision, etc. [2]. Therefore, identifying and compensating the kinematic parameter errors of the tandem robotic arm through kinematic calibration is of great significance to improve the absolute accuracy of the tandem robotic arm.

The main process of kinematics calibration is as follows: first, establish the kinematic model of the tandem robotic arm, including the kinematic forward solution model and the kinematic inverse solution model, then analyze the kinematic parameter error in the

model and establish the functional relationship between the kinematic parameter error and the EE pose error of the tandem robotic arm; second, the appropriate measurement scheme is determined according to the function model to obtain the EE pose error of the tandem robotic arm; third, the EE pose error is brought into the function model to solve the kinematic parameter error; finally, a joint driving angle solution strategy is established for the positive kinematics model with errors. The above four steps are called kinematic modeling, EE pose measurement, kinematic parameter identification and error compensation [3]. In the following section, the research status of each step will be introduced and an appropriate scheme will be proposed according to the characteristics of the tandem robotic arm used in this experiment.

Kinematic modeling: The essence of kinematic modeling is to establish the transformation matrix relationship between each coordinate system of the tandem robotic arm and the EE of the tandem robotic arm. It is the premise and basis for parameter identification. The model generally requires integrity, continuity, and parametric minima [4]. The most basic and typical kinematic model is the Denavit–Hartenberg (D-H) model [5]. The model uses four parameters to describe the kinematic parameters between adjacent joints, but when the adjacent joints are parallel or nearly parallel, the D-H model is discontinuous. Hayati [6], Veitschegger [7] et al. proposed a modified D-H model (MDH), adding a rotation around the y-axis between adjacent parallel axes in the D-H model to describe the non-parallelism of the two axes, solving the singularity problem of the D-H model. Stone proposed the S model of the three-translation and three-rotation 6-parameter model, which uses six parameters to describe the spatial transformation relationship between adjacent links. Compared with the D-H model, it is more intuitive, but it is not convenient for error compensation [8]. Zhuang and Rot proposed a 4-parameter CPC model and a 6-parameter MCPC model with three translations and one rotation in 1992. The CPC model is named for its “Complete and Parametrically Continuous” properties; the MCPC model is the modified CPC model. The continuity of the model is ensured by increasing the kinematic parameters. Since its coordinate changes are relatively gentle, it will not cause the sudden change of the pose of the tandem robotic arm [9]. Lv et al. established the forward kinematics model of the serial manipulator by using the screw method and verified its correctness using ADAMS software simulation. Compared to the D-H method, the screw method only needs to establish a tool coordinate system and a base coordinate system, which is simpler and more intuitive [10]. Chen et al. proposed a POE exponential product model (Product of Exponentials) based on the screw theory for the modular tandem robotic arm [11]. The POE model avoids the influence of the error caused by the transformation matrix on the calibration accuracy and makes the experimental process simpler. However, the calibration results of this method cannot be directly compensated to the tandem robotic arm control system and can only be converted into a D-H model first; in addition, the Jacobian matrix is difficult to solve, so the numerical solution can only be obtained by an iterative method.

EE pose measurement: There are various methods for measuring the EE pose of the tandem robotic arm, including laser interferometer, three-coordinate measuring instrument, telescopic ball bar, industrial camera, etc. Jian et al. [12] used a laser tracker to measure the five-degree-of-freedom tandem robotic arm for parameter identification and correction. The experimental results show that the compensation error has a significant effect. Xie et al. [13] used the linear structured light measurement system installed on the EE as a tool to obtain the three-dimensional coordinate information of the standard sphere center, established an error model according to the invariance principle of the spherical center coordinate in the basic coordinate system, and completed the calibration study of the tandem robotic arm. Wang [14] obtained the visual features of the robotic arm operation trajectory through hand eye calibration and the least squares method, achieving end pose monitoring. The final experiment showed that this method can effectively reduce pose and height errors. Yang et al. proposed a dynamic angle correction scheme that uses Creafom’s C-Track780 optical coordinate measuring machine to measure angle information online as feedback to accurately guide the end link of the tandem robotic arm to reach the expected

spatial coordinate point [15]. Legnani et al. developed a line sensor-based measurement platform system and applied it to an anthropomorphic tandem robotic arm by obtaining isotropic precision and high sensitivity, then using the same measurement system to perform calibration experiments [16]. Using three airborne cameras and relying on a coupled model combining kinematics and photogrammetry, Aitor proposed an analytical method to estimate the uncertainty of certain kinematic parameters, thereby enabling the transition from qualitative to observability to quantitative. Evaluation therefore becomes possible, and calibration of the tandem robotic arm is completed [17]. Jiang et al. used deep learning methods to establish neural network structures related to measurement and theoretical pose, and the predicted accuracy after training is comparable to the ranging accuracy of laser trackers [18]. Lu Yi and others completed the calibration of an Advantech LNC-S600 robot based on the linear structured light sensor; the average position error was reduced from 1.7256 mm to 0.3412 mm [19]. Luo Zhenjun et al. completed the calibration of the stacking robot based on a wire displacement sensor [20]. Balanji H. M. et al. calibrated the robot using a monocular camera; after calibration, the absolute position error and direction error of the robot converged to 2.5 mm and 0.2° , respectively [21]. Rozlivek J. et al. used a binocular camera to identify the pose information of the marked object fixed on the end effector of the multi chain robot and obtained the pose information of the multi chain robot, completing the error identification of the multi chain robot [22]. The above EE pose measurement methods have all been successfully applied in the kinematics calibration of tandem robotic arms, and each has its own advantages and disadvantages. For example, laser trackers and three-coordinate measuring instruments have high precision, but their cost is high, the measurement time is long, and this measurement method usually requires other auxiliary tools to be installed at the EE of the tandem robotic arm; despite this, the accuracy of the end auxiliary tools is often far superior. The measurement accuracy is lower than that of the laser tracker and the three-coordinate measuring instrument, resulting in redundant measurement accuracy. The visual measurement method needs to understand the principle of visual measurement, but the cost is cheap, and as a non-contact measurement tool, its measurement is more convenient and more efficient.

Parameter identification and error compensation: The process of parameter identification and error compensation is essential to solve the problem of optimal parameter error under constraint conditions and to compensate the optimal parameter error to the tandem robotic arm control system. Li et al. [23] proposed a calibration method of the manipulator by combining a Kalman filter and quadratic interpolation beetle antenna search algorithm; this combination can search the optimal motion parameters. Experiments show that this method has high calibration accuracy. Wang et al. [24] used the matrix method to analyze the calibration error model of kinematics parameters and added incremental error compensation; this can improve the accuracy of the manipulator. Urrea et al. [25] used the least squares method to simulate the 3-degree-of-freedom selective flexible assembly tandem robotic arm SCARA, obtained the algorithm performance index capable of parameter identification, and obtained a higher-precision end pose through error compensation. To reduce the influence of measurement noise and improve the calibration performance, Chen et al. [26] proposed an improved full-pose measurement and recognition optimization method. The method is based on the adaptive particle swarm optimization algorithm, has observable indicators and identification accuracy indicators, and considers external constraints, namely structural interference, and angle constraints; the simulation results show that the proposed error model has 36 error parameters, and has good stability. Dolinsky [27] introduced an inverse static kinematics calibration technique based on genetic programming, which is used to establish and identify model structure and parameters; this avoids the problems of traditional calibration methods and has the potential to identify real calibration models. Lattanzi et al. [28] developed a new geometric identification program for two kinds of industrial manipulators. The program allows the modification of the theoretical values of robot kinematics parameters. Experiments have proved the effectiveness of the geometric calibration method. Shi [29] et al. used a binocu-

lar vision system to measure the end position of the manipulator, established theoretical and actual distance error function, and used particle swarm optimization to solve the kinematics parameter errors and compensate for them. Finally, the absolute accuracy of the manipulator was significantly improved. Xing et al. [30] combined spin theory and the exponential product method to establish a distance error model for a UR10 robotic arm. The structural parameters were calibrated using a laser tracker on an experimental platform, and the local accuracy error was less than 1 mm. The Levenberg Marquardt (LM) algorithm [31] is a widely used improved least squares method that combines the gradient method and the Gaussian Newton method and has high robustness. Zhao [32] used an LM algorithm to complete parameter identification for the Eft ER50 robot; after calibration, its average position error was reduced from 2.038 mm to 0.136 mm. Chen [33] used a monocular camera and a standard sphere as tools to solve the identification equation using the first-order difference quotient method and completed the robot calibration based on point and distance constraints. Nguyen, H. N. et al. [34] used artificial neural networks to compensate for robot position errors caused by non-geometric errors and applied this method to the experimental calibration of the HH880 robot. The calibrated robot position accuracy has been effectively improved. Yan [35] used vector matrix analysis to obtain the mapping relationship between attitude error and structural parameter error and used a genetic algorithm to optimize the attitude accuracy of parallel robots. Finally, the simulation results show that, when compared with the least square method, the error identification algorithm of robot kinematics parameters based on genetic algorithm has obvious advantages. Kosmatopoulos et al. [36] solved the identification problem of manipulators using dynamic neural networks, and proposed a dynamic back-propagation scheme that can learn and identify nonlinear systems without requiring prior knowledge of the system for identification. This method can handle the sudden change of input data, the error convergence progress is fast, and, even when the input waveform does not appear, the network can still operate effectively after training.

However, there are still problems with the current research on calibration methods for robotic arms. At present, most of the robot kinematics parameter calibration methods use the joint length parameter and angle parameter identification method at the same time. Although a calibration method that only introduces position constraints can improve the positioning accuracy of the robot to a certain extent, it does not include angle accuracy as an evaluation indicator of the calibration results, and therefore cannot guarantee high angle accuracy. The angle error is usually smaller than the position error, and when measuring the pose error, the angle error is easily drowned out, resulting in poor calibration results. In addition, when using the least squares method for parameter identification, the identification equation is prone to pathological problems. Therefore, error identification will be affected, and compensation accuracy will also decrease.

In this paper, in view of the excellent characteristics of binocular vision that can obtain the full pose of the EE of the tandem robotic arm, and its low measurement cost, simple measurement and high efficiency, binocular vision is used to measure the pose of the EE of the tandem manipulator. Three ceramic standard spheres were used as measurement markers, and the EE pose of the tandem robotic arm was obtained in combination with the self-designed supporting measurement aids. At the same time, the MDH model (Modify-DH) solves the discontinuity problem of the D-H model and allows the obtained kinematic parameter errors to be easily compensated into the control system of the tandem robotic arm. The kinematics model in this paper selects the MDH model for modeling; based on the kinematic parameters of the tandem robotic arm corner control method, an error compensation strategy is established. Through the analysis of the error mapping model, it is found that the length parameter error has no effect on the end angle error, and the angle joint parameters and the length joint parameters are separated and calibrated; in addition, this article cites an ill-conditioned optimization method based on spectral correction iterative method, which completes parameter identification.

Compared to previous research, this article proposes new methods to solve existing problems. First, aiming at the problem of poor absolute accuracy of tandem robotic arms, a separation calibration scheme for kinematic parameter errors is formulated based on binocular vision, which improves the absolute position accuracy and absolute angle accuracy of tandem robotic arms. Second, aiming at the problem that the identification equation is prone to be ill-conditioned, an ill-conditioned optimization method based on the spectral correction method is adopted to make the error identification and compensation more accurate.

The structure of this paper is as follows. The introduction describes the research background and research status of this paper. In the first section, the kinematics modeling of the 6R series manipulator is carried out, including the positive and inverse kinematics solutions and the mapping relationship between the pose error of the end-effector of the serial manipulator. Next, according to the established error mapping relationship, the joint angle parameter error and the length parameter error are separated, and the pose constraint scheme and distance constraint scheme are established. Finally, the identification equation is optimized. The second section discusses the measurement principle of binocular stereo vision and the setting of measurement markers. The third section carries out the simulation experiment and the real machine experiment of the serial manipulator and discusses the experimental results. The conclusion part summarizes the research content and significance of this paper and proposes future research directions.

2. Methods

2.1. Geometric Error Identification

In this section, based on the theoretical kinematic parameters of the tandem robotic arm, the kinematics forward and inverse solution models are established. According to the positive kinematics solution, from the perspective of differential motion, the mapping relationship between the pose error of the tandem robotic arm and the joint parameter error is established. By analyzing the error mapping relationship, a method to separate and calibrate the joint angle parameter error and joint length parameter error is proposed. According to this relationship, the angle constraints and distance constraints of the end of the tandem robotic arm are established, and optimization is made for the ill-conditioned situation of the identification equation.

2.1.1. Robotic Arm Kinematics Model

The tandem robotic arm used in this paper is the IRB-1200 from ABB, as shown in Figure 1.

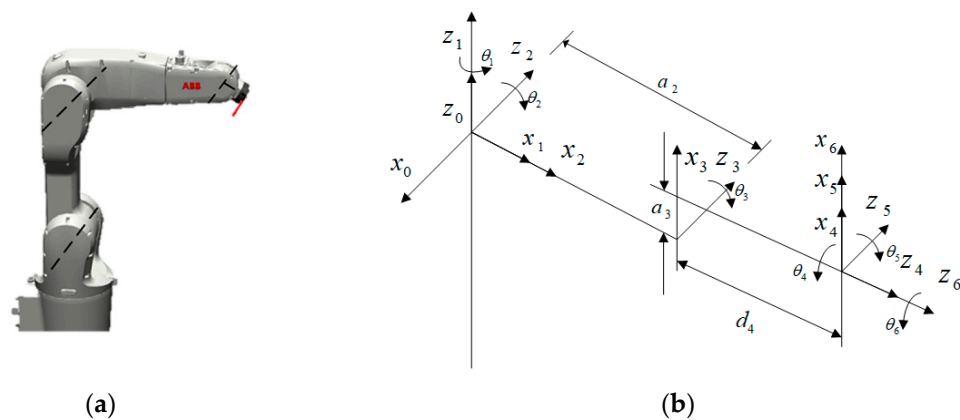


Figure 1. (a) 3D model of IRB-1200; (b) modeling of each joint.

Since the axes of the second and third joint axes of the series manipulator are parallel, to ensure model continuity, the MDH model is used in this paper. The MDH model is based on the D-H model by adding a parameter β that rotates around the y-axis to the joint

parameters to replace the joint parameter d that undergoes a jump to ensure the continuity of the model. The transformation relationship between the adjacent link coordinate systems is shown in Formula (1):

$${}_{i+1}^i T = \text{rot}(x_i, \alpha_i) \text{trans}(x_i, a_i) \text{trans}(z'_{i+1}, d_i) \text{rot}(z'_{i+1}, \theta_i) \text{rot}(y_{i+1}, \beta_i) \tag{1}$$

The transformation matrix of each joint is multiplied in turn to obtain the pose transformation matrix from the base coordinate system of the tandem robotic arm to the end flange coordinate system.

$$T = {}_6^0 T = {}_1^0 T {}_2^1 T {}_3^2 T {}_4^3 T {}_5^4 T {}_6^5 T \tag{2}$$

The last three joint axes of the tandem robotic arm intersect at one point. Currently, the rotation angles of the first three joint axes determine the position of the reference point of the EE of the tandem robotic arm, and the rotation angles of the last three joint axes determine the posture of the EE of the tandem robotic arm to execute its reference point. The inverse kinematics solution of the tandem robotic arm is divided into two parts, the inverse position solution and the inverse angle solution, by using the method of pose separation.

The first is the position inverse solution. The three joint axes of the tandem robotic arm intersect at one point, and the origins of the link coordinate systems {4}, {5}, {6} are all set at this intersection. Therefore, in the base coordinate system {0}, the description of the origin of the coordinate systems {4}, {5}, {6} is the same, i.e.,

$${}^0 P_{40} = {}^0 P_{50} = {}^0 P_{60} \tag{3}$$

From the transformation matrix ${}^3_4 T(\theta_4)$, it is easy to obtain the description of the origin of the coordinate system {4} in the coordinate system {3} as ${}^3 P_{40} = [a_3, d_4, 0, 1]^T$, and then obtain its description in the basic coordinate system {0}:

$${}^0 P_{40} = {}^0_1 T(\theta_1) {}^1_2 T(\theta_2) {}^2_3 T(\theta_3) {}^3 P_{40} \tag{4}$$

Substitute ${}^2_3 T(\theta_3)$, ${}^1_2 T(\theta_2)$, ${}^0_1 T(\theta_1)$ into Equation (5) to get:

$${}^0 P_{40} = [c_1 v_1, s_1 v_1, v_2, 1]^T \tag{5}$$

in: $v_1 = c_2 u_1 - s_2 u_2, v_2 = -s_2 u_1 - c_2 u_2$

$$u_1 = a_3 c_3 - d_4 s_3, u_2 = a_3 s_3 + d_4 c_3 \tag{6}$$

in: $c_1 = \cos \theta_1, s_1 = \sin \theta_1, c_2, s_2, c_3, s_3$, similarly.

Because in the inverse kinematics solution of the manipulator, the position of the EE reference point and the posture of the EE effector are given, combine with ${}^0 P_{60} = [p_x, p_y, p_z, 1]^T$ Equation (5) to get the equation:

$$[c_1 v_1, s_1 v_1, v_2, 1]^T = [p_x, p_y, p_z, 1]^T \tag{7}$$

From the square of the distance from the origin, we can get: $v_1^2 + v_2^2 = p_x^2 + p_y^2 + p_z^2$, substitute (7), using trigonometric substitution, we get:

$$\theta_3 = \arctan 2(a_3, d_4) - \arctan 2\left(k, \pm \sqrt{a_3^2 + d_4^2 - k^2}\right) \tag{8}$$

in: $k = \frac{p_x^2 + p_y^2 + p_z^2 - a_2^2 - a_3^2 - d_4^2}{2a_2}$

After obtaining θ_3 , it can be substituted into Formula (6) to obtain u_1, u_2 , and then there are:

$$s_2 u_1 + c_2 u_2 = -p_z \tag{9}$$

Introducing triangular substitution as above to get:

$$\theta_2 = \arctan2\left(-p_z, \pm\sqrt{u_1^2 + u_2^2 - p_z^2}\right) - \arctan2(u_1, u_2) \tag{10}$$

Substitute u_1, u_2, θ_2 into Formula (6) to obtain v_1 , and then into Formula (7) to obtain:

$$\begin{cases} \theta_1 = \arctan2(p_y, p_x) v_1 > 0; \\ \theta_1 = \arctan2(-p_y, -p_x) v_1 < 0; \end{cases} \tag{11}$$

Then there is the angle inverse solution. It is easy to see from ${}^0P_{40} = {}^0P_{50} = {}^0P_{60}$ the above solution that is only related to $\theta_1, \theta_2, \theta_3$, and solving can only be based on to establish an effective equation to solve. From:

$${}^3R = {}^0R^{-1} {}^0R = {}^0R^T {}^0R \tag{12}$$

From this you can get the equation: $c_5 = -a_x c_1 s_{23} - a_y s_1 s_{23} - a_z c_{23}$;
Therefore:

$$\theta_5 = \arctan2\left(\pm\sqrt{1 - c_5^2}, c_5\right) \tag{13}$$

From this, two equations can be obtained:

$$\begin{cases} -c_4 s_5 = a_x c_1 c_{23} + a_y s_1 c_{23} - a_z s_{23} \\ s_4 s_5 = -a_x s_1 + a_y c_1 \\ c_6 s_5 = -n_x c_1 s_{23} - n_y s_1 s_{23} - n_z c_{23} \\ -s_6 s_5 = -o_x c_1 s_{23} - o_z c_{23} \end{cases} \tag{14}$$

When $s_5 > 0$,

$$\begin{aligned} \theta_4 &= \arctan2(-a_x s_1 + a_y c_1, -a_x c_1 c_{23} - a_y s_1 s_{23} + a_z s_{23}); \\ \theta_6 &= \arctan2(o_x c_1 s_{23} + o_y s_1 s_{23} + o_z c_{23}, -n_x c_1 s_{23} - n_y s_1 s_{23} - n_z c_{23}); \end{aligned} \tag{15}$$

When $s_5 < 0$,

$$\begin{aligned} \theta_4 &= \arctan2(a_x s_1 - a_y c_1, a_x c_1 c_{23} + a_y s_1 s_{23} + a_z s_{23}); \\ \theta_6 &= \arctan2(-o_x c_1 s_{23} - o_y s_1 s_{23} - o_z c_{23}, n_x c_1 s_{23} + n_y s_1 s_{23} + n_z c_{23}); \end{aligned} \tag{16}$$

The two sets of values θ_4, θ_6 are exactly different π .
in: $c_{23} = \cos(\theta_2 + \theta_3), s_{23} = \sin(\theta_2 + \theta_3)$ and so on.

2.1.2. Error Mapping Model

The EE pose error caused by the kinematic parameter error can be approximated by the following formula:

$$d_{i+1}^i T = \frac{\partial {}^i T_{i+1}}{\partial \theta_i} \delta \theta_i + \frac{\partial {}^i T_{i+1}}{\partial d_i} \delta d_i + \frac{\partial {}^i T_{i+1}}{\partial a_i} \delta a_i + \frac{\partial {}^i T_{i+1}}{\partial \alpha_i} \delta \alpha_i + \frac{\partial {}^i T_{i+1}}{\partial \beta_i} \delta \beta_i = \delta_{i+1}^i T \cdot {}^i T_{i+1} \tag{17}$$

In the above formula $\delta \theta_i, \delta d_i, \delta a_i, \delta \alpha_i, \delta \beta_i$ are the structural parameter error of joint i , $\delta_{i+1}^i T$ is the differential transformation matrix, and $d_{i+1}^i T$ is the single joint pose error caused by the joint i parameter error. Convert this error to the end of the tandem robotic arm and convert all joints. The resulting end pose errors are accumulated together to produce:

$${}^0T + d_6^0 T = \prod_{i=0}^6 \left({}^i T_{i+1} + d_{i+1}^i T \right) \tag{18}$$

Expanding Equation (18) and ignoring higher-order infinitesimal terms, we get:

$$d_6^0T = \left(\sum_{i=0}^6 {}^0T_i \cdot \delta_{i+1} {}^i T_i \cdot {}^0T \right) \cdot {}^0T \quad (19)$$

The mapping relationship between the end error of the tandem robotic arm and the structural parameter error can be described as:

$$\Delta e = J \cdot q \quad (20)$$

Among them: $\Delta e = [d_x \ d_y \ d_z \ \delta_x \ \delta_y \ \delta_z]^T$, which is the pose error of the end of the tandem robotic arm in Cartesian space, where the first three rows of elements are the position errors and the last three rows of elements are the angle errors. J is the Jacobian matrix, which is only affected by the kinematic parameters of the tandem robotic arm, q is the parameter error vector composed of $\delta\theta$, δd , δa , $\delta\alpha$, and $\delta\beta$; each contains six parameters except for $\delta\beta$ with only one parameter $\delta\beta_2$. Since only joint 2 and joint 3 are parallel, and $\delta\beta_2$ is not 0, the others are 0, so only need to identify. The motion error model of the tandem robotic arm reflects the mapping relationship between the pose error of the EE of the tandem robotic arm and the error of the joint structure parameters and is the basis for kinematic parameter identification based on the difference between the theoretical pose and the actual pose of the tandem robotic arm.

2.1.3. Joint Parameter Error Separation

Under some specific physical constraints, not all joint parameter errors can be identified; these unidentifiable parameters are called redundant parameters. If the redundant parameters are not eliminated during the identification process, the identification accuracy will be greatly affected. The redundant parameters can be divided into two categories. The first category is called the parameters that have no effect on the terminal pose error, because the columns in the error mapping matrix J corresponding to these error parameters are all zero, which has no effect on the terminal pose. The second category is related parameters, which often refer to multiple joint parameters, and their corresponding columns in the error mapping matrix J show a linear correlation. By analyzing the last three rows of angle error mapping matrices in Equation (20), it is found that all the columns in the angle error mapping corresponding to the link length a , and that the joint distance d is zero, which indicates that the joint length parameter has a significant effect on the terminal angle. Based on this phenomenon, the joint angle parameter error and joint parameter error can be calibrated separately. That is, the identification of joint angle parameters is completed based on angle constraints, and then the identification of joint length parameter errors is completed based on distance constraints.

After removing the joint length parameters and the columns in the corresponding angle error mapping matrix, the angle error mapping matrix is decomposed by QR, and it is found that the diagonal element of the sixth row in the matrix R is 0, which corresponds to the third joint rotation angle θ_3 of the robot. It is a redundant parameter and cannot be identified by the method of pose constraint. By analyzing the angle error mapping matrix, we found that the θ_3 corresponding column and the θ_2 corresponding column are actually and linearly correlated. By analyzing the geometric structure of the robot, since the axes of the 2 and 3 joints are theoretically parallel, when a $-\Delta$ angle error occurs and a $+\Delta$ angle error occurs, the front and rear joint axes of the fourth axis of the robot are parallel; that is, the EE pose remains unchanged. As shown in Figure 2, Figure 2a is a schematic diagram of the robotic arm, and Figure 2b is a calculation schematic diagram. So only the sum of two joint angle errors can be identified through the pose constraint. The two corner errors cannot be identified separately. However, the motion errors of the above two corners will affect the end position, and the combination of position constraints and angle constraints can complete the identification of the two corner errors.

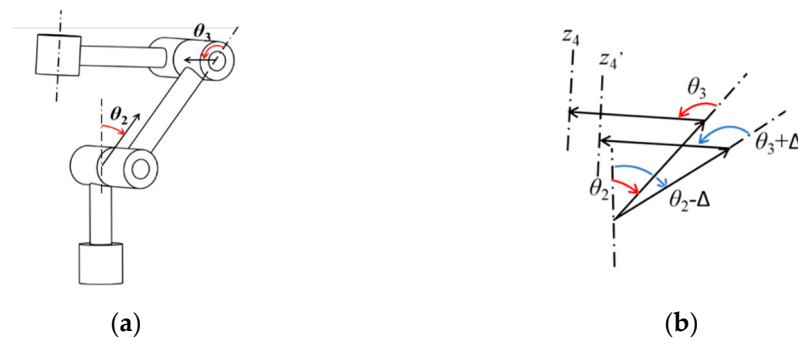


Figure 2. Redundancy relationship between the second and third joint angles. (a) Schematic diagram of the robotic arm. (b) Calculation schematic diagram.

Therefore, the final parameters to be identified in the parameter identification experiment based on angle constraints are determined as follows:

$$q = [\delta\theta_1 \ \delta\alpha_1 \ \Delta\theta_2 \ \delta\alpha_2 \ \delta\beta \ \delta\alpha_3 \ \delta\theta_4 \ \delta\alpha_4 \ \delta\theta_5 \ \delta\alpha_5 \ \delta\theta_6 \ \delta\alpha_6]^T \tag{21}$$

in: $\Delta\theta_2 = \delta\theta_2 + \delta\theta_3$

The final parameters to be identified in the parameter identification experiment based on distance constraints are as follows:

$$q = [\delta d_1 \ \delta a_1 \ \delta d_2 \ \delta a_2 \ \delta d_3 \ \delta a_3 \ \delta d_4 \ \delta a_4 \ \delta d_5 \ \delta a_5 \ \delta d_6 \ \delta a_6 \ \delta\theta_2 \ \delta\theta_3]^T \tag{22}$$

2.1.4. Angle Constraints and Distance Constraints

Record θ_i^N as the nominal state vector of the measurement point in the coordinate system of the tandem robotic arm; if θ_j^N is the nominal angle vector after the tandem robotic arm moves a certain angle, then the nominal motion angle of the tandem robotic arm is $\Delta\theta_{ij}^N = \theta_j^N - \theta_i^N$, and θ_i^R is the actual angle of the measurement point before the angle movement. If the vector θ_j^R is the actual state vector of the measurement point after the angle movement then the actual movement angle of the tandem robotic arm is $\Delta\theta_{ij}^R = \theta_j^R - \theta_i^R$, and the motion angle error of the tandem robotic arm $\Delta\theta$ can be expressed as:

$$\Delta\theta = \Delta\theta_{ij}^R - \Delta\theta_{ij}^N \tag{23}$$

where $\Delta\theta = [\Delta\theta_x \ \Delta\theta_y \ \Delta\theta_z]^T$, is the three-dimensional Cartesian angle error.

From Equation (20), it can be known that the actual posture θ_1^R, θ_j^R of the two measurement points can be expressed by the following equation:

$$\begin{aligned} \theta_1^R &= \theta_1^N + J_{3\sim 6} \cdot q \\ \theta_j^R &= \theta_j^N + J_{3\sim 6} \cdot q \end{aligned} \tag{24}$$

Being like the definition of distance, we try to find the minimum sum of angle errors in the x, y, z directions between two points. We define an angle error metric $d\theta$, which can be defined as follows:

$$d\theta = \left\| \Delta\theta_{ij}^R - \Delta\theta_{ij}^N \right\|_2 = \sqrt{(\Delta\theta_x^R - \Delta\theta_x^N)^2 + (\Delta\theta_y^R - \Delta\theta_y^N)^2 + (\Delta\theta_z^R - \Delta\theta_z^N)^2} \tag{25}$$

It is recorded $F_{Euler}(P, A)$ as the function of the forward kinematics of the tandem robotic arm to solve the Euler angle of the end angle, where P is the D-H parameter of the tandem robotic arm and A is the rotation angle of each joint, then the Euler angle of the measurement point in the coordinate system of the tandem robotic arm can be expressed for:

$$\theta = F_{Euler}(P, A) \tag{26}$$

Then the angel constraint equation can be expressed as:

$$\min \Delta \theta = \left\| (F_{\text{Euler}}(P, A_i) + J_{4 \sim 6} q) - ((F_{\text{Euler}}(P, A_j) + J_{4 \sim 6} q) - \Delta \theta_{ij}^R) \right\|^2 \tag{27}$$

Denote p_i^N, p_j^N , as the nominal coordinate vector of the two measurement points in the coordinate system of the tandem robotic arm; the distance between the two can be expressed as:

$$d_{ij}^N = \|p_i^N - p_j^N\|_2 = \sqrt{(p_{xi}^N - p_{xj}^N)^2 + (p_{yi}^N - p_{yj}^N)^2 + (p_{zi}^N - p_{zj}^N)^2} \tag{28}$$

From Equation (20), it can be known that the actual coordinates of the two measurement points p_i^R, p_j^R , i.e.,

$$\begin{aligned} p_i^R &= p_i^N + J_{1 \sim 3} q \\ p_j^R &= p_j^N + J_{1 \sim 3} q \end{aligned} \tag{29}$$

Then the distance constraint equation is:

$$\min \Delta d = \left(\| (F_{\text{dis}}(JP, JA_i) + J_{1 \sim 3} q) - (F_{\text{dis}}(JP, JA_j) + J_{1 \sim 3} q) \|_2 - d_{ij}^R \right)^2 \tag{30}$$

2.1.5. Identification Equation Optimization

When solving the minimum pose constraint, it is necessary to measure the error of n groups of EEs poses and construct the following identification equations for iterative solution.

$$e = Hq \tag{31}$$

In: $e = [e_1 \ e_2 \ \dots \ e_n]^T$, $H = [J_1 \ J_2 \ \dots \ J_n]^T$, rewriting it into an extended Jacobian matrix form, the joint parameter error q can be expressed as:

$$q = (H^T H)^{-1} H^T e \tag{32}$$

It can be seen from the above formula that to identify q, it is necessary to ensure that $H^T H$ is reversible; this requires that the parameters to be identified must be independent, and a reasonable pose must be selected to measure enough data. Here, $H^T H$, when the matrix is inverted, an ill-conditioned problem is generally caused, $(H^T H)^{-1}$ is mainly manifested in that the condition number of is much larger than 1, which makes the calculation error larger. Therefore, an improved spectral correction iterative method is proposed in this paper. The traditional spectral correction iterative method is as follows:

$$(H^T H)q = H^T e \tag{33}$$

Add an estimated value of q to both the left and right sides of the above equation $\hat{\Delta}q$, available:

$$(H^T H + I) \cdot \hat{\Delta}q = H^T \cdot e + \hat{\Delta}q \tag{34}$$

After shifting the term, since both sides contain $\hat{\Delta}q$, it must to be solved according to the iterative method; the formula is:

$$\hat{\Delta}q^{(n)} = (H^T H + I)^{-1} (H^T \cdot e + \hat{\Delta}q^{(n-1)}) \tag{35}$$

or

$$\hat{\Delta}q^{(n)} = (a + a^2 + a^3 + \dots + a^n) H^T \cdot e + a^n \hat{\Delta}q^{(0)} \tag{36}$$

In: $\hat{\Delta q}^{(0)}$ is the initial value of $\hat{\Delta q}^{(n)}$, $a = (H^T H + I)^{-1}$.

The above is the classical spectrum correction iterative method. This method maintains the original equivalent relationship of the equation while introducing the bias term, so that the calculation result is unbiased. The algorithm uses the identity matrix as the bias term to reduce the condition number of a , and then estimates the true value of Δq .

2.2. Pose Measurement Based on Binocular Vision

2.2.1. The Principle of Binocular Vision Stereo Measurement

Binocular vision has the excellent characteristic of obtaining the three-dimensional position information of markers. The schematic diagram of binocular stereo vision measurement is shown in Figure 3.

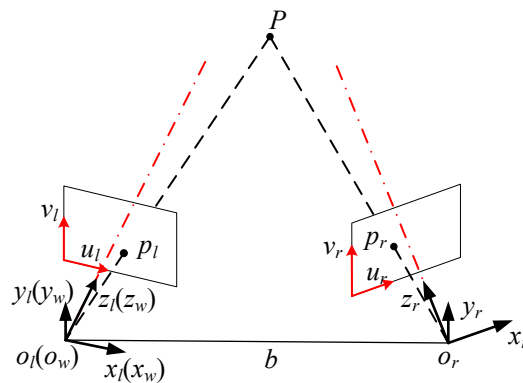


Figure 3. Binocular camera imaging model.

To obtain the three-dimensional information of the target point to be measured, a fixed coordinate system is required to provide a unified description of the left and right camera coordinate systems [37]. In the figure, $O_l X_l Y_l Z_l$ is the left camera coordinate system, $O_r X_r Y_r Z_r$ is the right camera coordinate system, $O_p X_p Y_p Z_p$ is the world coordinate system, and p is the measurement target point. If it is specified that the left camera coordinate system is the world coordinate system then the coordinate transformation matrix between the left camera coordinate system and the right camera can be represented by $[R_c \quad t_c]$, where R_c and t_c are the rotation matrix and translation vector of the left camera coordinate system relative to the right camera coordinate system, respectively. This is the extrinsic parameter of the binocular camera. According to the principle of pinhole imaging combined with the internal parameters of the binocular camera, the world coordinates of p in the left and right camera coordinate systems can be obtained. According to the coordinate uniqueness of point p in the world coordinate system, combined with the external parameters of the binocular camera, the three-dimensional coordinates of point p in the world coordinate system (i.e., the left camera coordinate system) can be obtained. The intrinsic and extrinsic parameters of the binocular camera can be obtained by camera calibration, where the internal parameter matrix is as in Formula (37).

$$K_l = \begin{bmatrix} f_{lx} & s_l & u_{l0} \\ 0 & f_{ly} & v_{l0} \\ 0 & 0 & 1 \end{bmatrix}, K_r = \begin{bmatrix} f_{rx} & s_r & u_{r0} \\ 0 & f_{ry} & v_{r0} \\ 0 & 0 & 1 \end{bmatrix} \tag{37}$$

2.2.2. Setting of Key Coordinate Systems and Measurement Markers

Based on the above binocular stereo vision, we devised the following scheme to measure the pose of the tandem robotic arm. In the measurement process, a 25.4 mm ceramic matte standard ball is used, and its shape accuracy is as high as 1 μ m. Three ceramic standard balls are installed on a high-precision calibration plate (Figure 4), and the

heights of the three standard balls are equal. Ensure that the centers of the three ceramic standard spheres are on a horizontal plane parallel to the plane of the calibration plate.



Figure 4. Calibration plate. (Physical image).

Install the calibration plate on the end of the tandem robotic arm; the calibration plate is precisely positioned at the end of the tandem robotic arm by positioning pins. The position of the pin hole is shown in Figure 5, and the position of the pin hole at the end of the serial robot arm and the coordinate system of the end flange are shown in Figure 6.

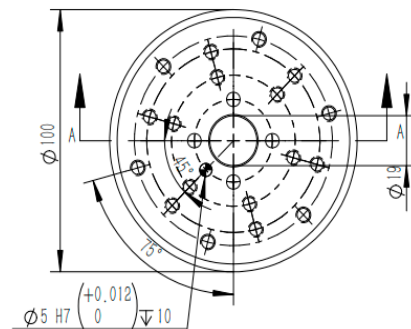


Figure 5. Calibration plate. (Vertical view).

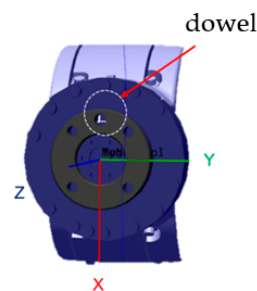


Figure 6. Flange at the end of the tandem robotic arm.

The X-axis direction of the EE flange coordinate system is collinear with the position of the pin. If a ceramic standard ball is placed on the opposite side of the pin hole, the center of the circumscribed circle determined by the center of the three standard balls is the same as the one mentioned above. The standard ball connection line is the X-axis direction, and the Z-axis direction is directed to the outside of the paper. According to the right-hand rule, the Y-axis direction can be determined. Through the above, we can determine the placement of the three ceramic standard balls so that the three the direction of the coordinate system determined by the center of the sphere is completely consistent with the direction of the coordinate system of the flange at the EE of the tandem robotic arm. The specific measurement scene and the way of establishing the spherical coordinate system are shown in Figure 7. Figure 7a shows the measurement scene and layout with a black board placed behind three standard balls. Due to the complex surrounding environment, this board can increase contrast ratio and enable the camera to better recognize ceramic standard balls.

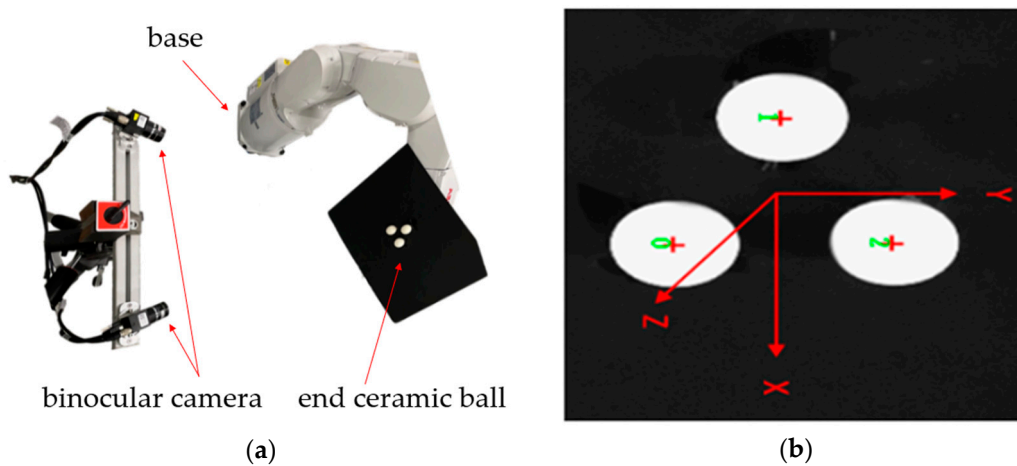


Figure 7. Schematic diagram of pose measurement. (a) Schematic diagram of pose measurement. (b) Image processing process.

The principle diagram of angle measurement of the robotic arm is shown in Figure 8. Let the coordinates of the three spherical centers be $p_0 = (x_0, y_0, z_0)^T$, $p_1 = (x_1, y_1, z_1)^T$, $p_2 = (x_2, y_2, z_2)^T$, respectively, and the coordinates of the center of the circumscribed circle fitted by the three spheres be $p_3 = (x_3, y_3, z_3)^T$. To ensure that the spherical coordinate system has the same posture as the coordinate system at the EE of the tandem robotic arm, we ensure the X-axis direction of the spherical coordinate system points runs from p_1 to p_3 . The Z-axis direction is pointed to the outside by the calibration plate, and the Y-axis direction is determined by the right-hand rule. Therefore, the directions of each coordinate axis of the spherical plane are:

$$\begin{cases} X = p_0 - p_1 \\ Z = (p_0 - p_1) \times (p_2 - p_1) \\ Y = Z \times X \end{cases} \quad (38)$$

convert it to a unit vector.

$$\begin{cases} x = X^T / \|X\| \\ y = Y^T / \|Y\| \\ z = Z^T / \|Z\| \end{cases} \quad (39)$$

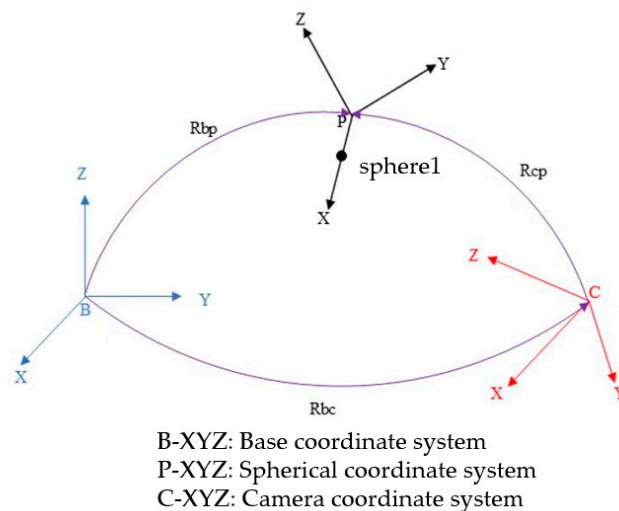


Figure 8. Principle diagram of angle measurement of tandem robotic arms.

Therefore, the angle transformation of the spherical plane coordinate system relative to the camera coordinate system is as follows:

$$R_{cp} = \begin{bmatrix} x(1) - y(1)z(1) \\ x(2) - y(2)z(2) \\ x(3) - y(3)z(3) \end{bmatrix} \tag{40}$$

Since the spherical coordinate system and the coordinate system of the end effector of the tandem robotic arm are coincident, the angle transformation between the spherical plane coordinate system and the base coordinate system of the tandem robotic arm follows:

$$R_{bp} = R_z \cdot R_y \cdot R_x \tag{41}$$

In the second measurement, the method of establishing the coordinate system is the same as that of the first system, so at the second position, the spherical coordinate system can be expressed as the base coordinate system of the series manipulator.

$$R'_{bp} = R_{bc} \cdot R_{cp} \tag{42}$$

Convert the angle matrix to the corresponding Euler angle to get the angle of the tandem robotic arm in the Cartesian coordinate system:

$$\begin{cases} R'_x = \text{atan2}(R'_{bp}(3,2), R'_{bp}(3,3)) \\ R'_y = \text{atan2}\left(-R'_{bp}(3,1), \sqrt{R'_{bp}(3,2)^2 + R'_{bp}(3,3)^2}\right) \\ R'_z = \text{atan2}(R'_{bp}(2,1), R'_{bp}(1,1)) \end{cases} \tag{43}$$

So far, we can get the measured value of the angle change of the end of the tandem robotic arm. In addition, since the calibration plate is fixed to the end effector of the tandem robotic arm, the moving distance of the ball is the moving distance of the end of the tandem robotic arm, and the position of the tandem robotic arm. Mobile information is also available.

2.3. Simulation Model Design

The model of the tandem robotic arm used in this paper is the IRB-1200 tandem robotic arm of ABB Company, and its theoretical joint parameters are shown in Table 1.

Table 1. Theoretical joint parameters of IRB-1200.

Joint i	$\theta/^\circ$	d/mm	a/mm	$\alpha/^\circ$	$\beta/^\circ$	$\theta_{\min}/^\circ$	$\theta_{\max}/^\circ$
1	0	0	0	0	-	-170	170
2	0	-	0	-90	0	-100	130
3	0	0	350	0	-	-200	70
4	0	351	42	-90	-	-270	270
5	0	0	0	90	-	-130	130
6	0	0	0	-20	-	-360	360

First, the angle parameter simulation identification experiment is carried out. The preset value of the angle parameter error in this experiment is shown in Table 2:

Table 2. Default identification joint parameter errors.

Joint <i>i</i>	$\theta/^\circ$	$\alpha/^\circ$	$\beta/^\circ$
1	0.07	0.1	-
2	-0.4	0.4	0.1
3	-	-0.5	-
4	0.11	0.2	-
5	-0.3	0.4	-
6	0.1	-0.5	-

Among them, the preset error of the joint angle θ_2 is the sum of $\delta\theta_2$ and $\delta\theta_3$.

The above joint errors are added to the theoretical joint parameters to obtain a kinematic model with structural parameter errors. The pose obtained by the kinematic model with errors is taken as the actual pose, the kinematic model determined by the theoretical joint parameters is taken as the theoretical pose, and simulation experiments are carried out. The experimental steps are as follows:

- (1) For the theoretical kinematics model, 50 groups of joint angle data of the beginning and end of the posture movement were obtained. Half of each joint's rotation angle data are used as the calibration set, and the other half are used as the compensation set. Denote the theoretical moving distance and theoretical motion posture obtained by calibrating the joint rotation angle of the set as A_1 .
- (2) Set the error value of each parameter, input the error value into the simulation model, and input the beginning and end joint rotation angle into the kinematic model with error to obtain the actual moving distance and motion posture. Record as A_2 .
- (3) Take A_1 and A_2 as input, bring into the identification equation established above, and calculate the joint parameter error in combination with the established angle constraints.
- (4) Compensate the calculated joint parameter errors into the theoretical kinematics model, input the beginning and end data of the joint rotation angle of the compensation set into the simulation model, and calculate the posture motion after compensation.
- (5) Compare the posture motion after compensation with the posture motion before compensation and determine the motion accuracy of the tandem robotic arm after compensation.

2.4. Tandem Robotic Arm Entity Experiment Design

The repeatability accuracy of the IRB-1200 tandem manipulator used in this paper is within 0.02 mm. Its absolute accuracy is not mentioned in the product manual. The binocular camera model is MV-EM500M, its highest resolution is 2592×1944 , and the pixel size is $2.2 \mu\text{m} \times 2.2 \mu\text{m}$. The resolution of the lens is 5M and the focal length is 16 mm. The dimensions of the calibration board are shown in Figure 9. This calibration board is different from the previous one, which is used to determine the internal parameters (such as distortion coefficient) and external parameters (such as pose between cameras) of the camera.

The size of the large circle is 6 mm, the size of the small circle is 3 mm, and the circle size accuracy and position accuracy are both μm level. The circles on the calibration board are coated with special reflective materials, and the rest are all coated with special absorbing materials, making the calibration board have high contrast, which is conducive to improving the calibration accuracy of the camera for binoculars.

The experimental steps are as follows:

- (1) Given different end poses, bring in an error-free theoretical kinematics positive solution model, and obtain the beginning and end rotation angles of each joint motion.

- (2) Control the movement of the tandem robotic arm to the beginning and end of each joint movement, and the binocular camera measures the actual movement distance and movement posture.
- (3) Execute the calibration procedure to obtain the joint parameter error of the tandem robotic arm and compensate the joint parameter error into the theoretical kinematics model of the tandem robotic arm and obtain the actual motion end angle of each joint through the actual inverse solution.
- (4) Control the movement of the tandem robotic arm to the actual movement end angle of each joint, and the binocular camera measures the movement distance and movement posture of the end after compensation.
- (5) Compare the end pose error values before and after compensation.

The solution process of the above actual inverse solution is as follows:

- (1) Knowing each joint parameter P and the theoretical pose of the tandem robotic arm C_t in the Cartesian coordinate system, the initial joint rotation angle A_0 is obtained from the theoretical inverse solution in Section 2.1.1.
- (2) Bring A_0 into the kinematic model with error to obtain the actual pose of C_r the tandem robotic arm.
- (3) Calculate the amount of change in the end pose caused by the joint angle increasing by one step and obtain the mapping function between the joint angle increasing by one step and the end pose transformation.
- (4) Calculate the change amount of the joint rotation angle through the difference between the actual pose and the theoretical pose and bring it into the mapping function in step (3) to obtain the increase value of the joint rotation angle.
- (5) Bring the obtained joint angle into the kinematics model with error, get a set of poses C_i compare C_i the C_r sum, if the calculation accuracy is satisfied, output the actual pose of each joint angle; if not, put as the initial pose, repeat steps (3) to (5) until the calculation accuracy is satisfied.

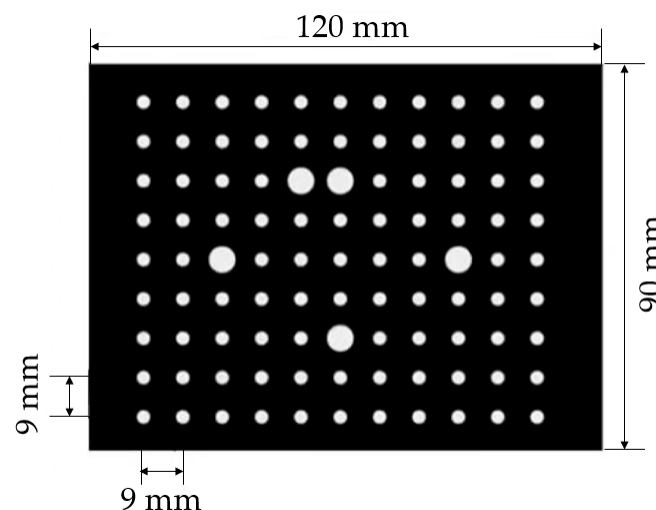


Figure 9. Calibration board for camera calibration.

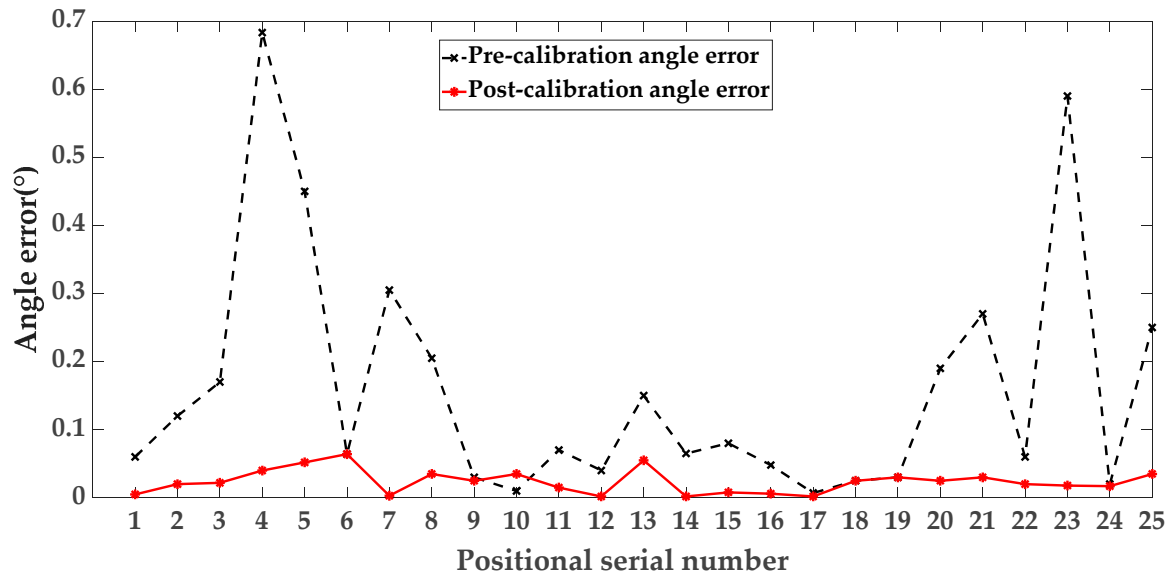
3. Results

3.1. Simulation Model Results

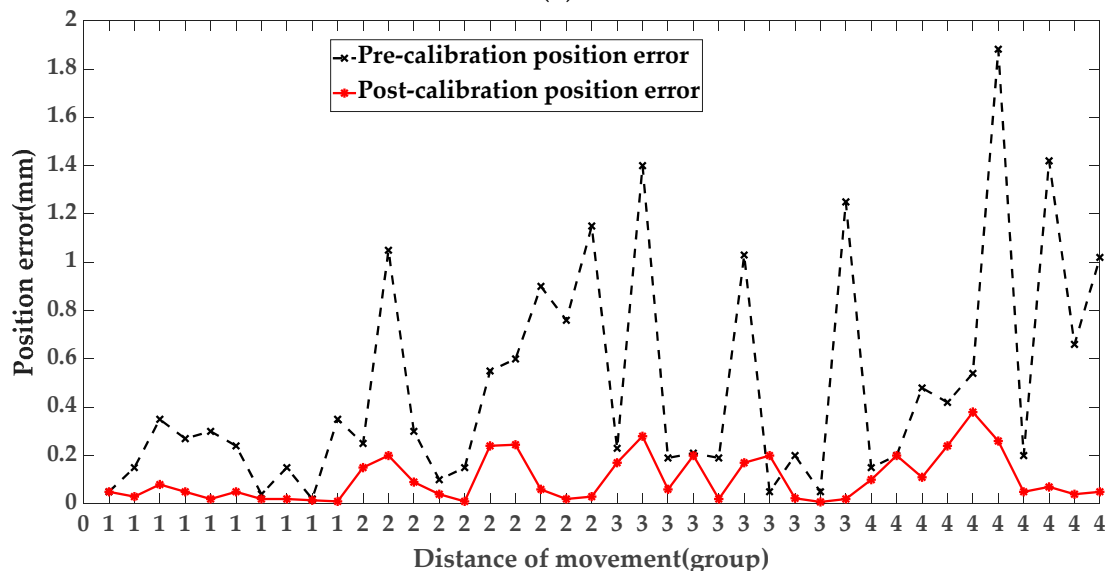
Carry out the above simulation experiments, combined with the accuracy of the measurement system, add random errors obeying the $N(0, 0.01^2)$ distribution to the measurement data. The obtained identification results are shown in Table 3, and the calibrated accuracy is shown in Figures 10 and 11.

Table 3. The identified joint parameter errors.

Joint i	$\theta/^\circ$	$\alpha/^\circ$	$\beta/^\circ$
1	0.0560	0.0373	-
2	-0.4227	0.4190	0.0770
3	-	-0.6423	-
4	0.1887	0.2496	-
5	-0.3051	0.3445	-
6	0.1006	-0.4000	-

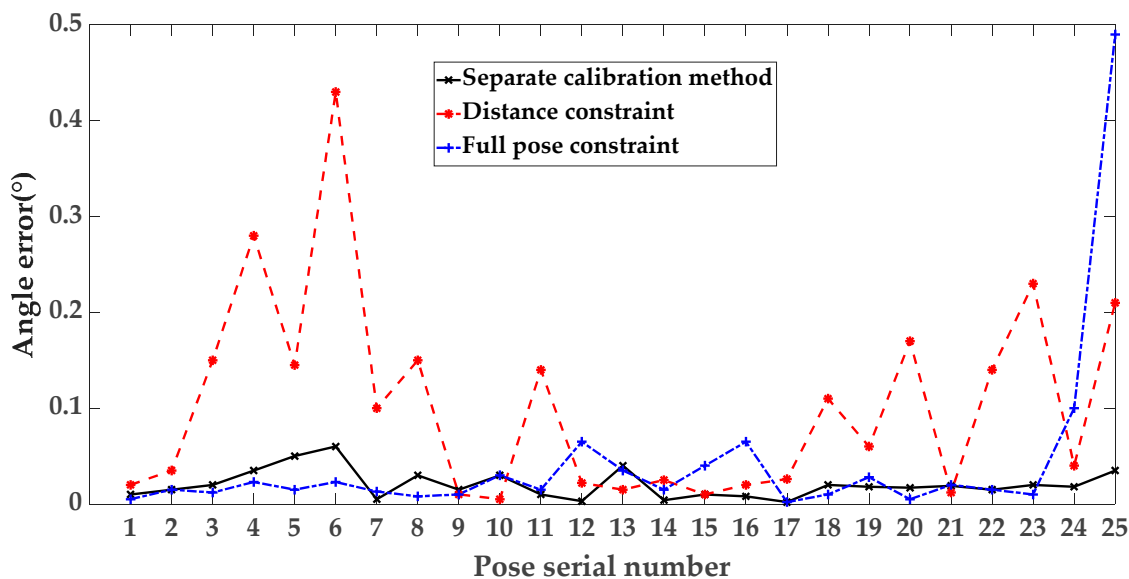


(a)

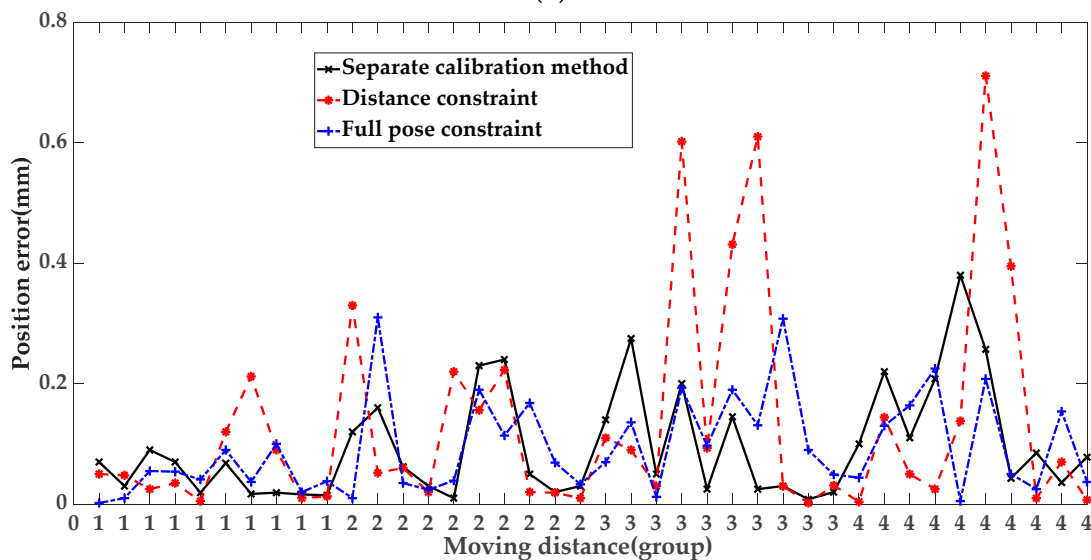


(b)

Figure 10. The posture error of the robot before and after the calibration. (a) Compensate for the angle error of the front and rear robots. (b) Compensate for the position error of the front and rear robots.



(a)



(b)

Figure 11. Error comparison of three methods. (a) Comparison of angle error of three methods. (b) Comparison of the position error of the three methods.

Next, the remaining joint parameter errors are identified by combining the distance constraints. The remaining joint parameter errors are shown in Table 4:

Table 4. Default identification joint parameter errors.

Joint i	$\theta/^\circ$	d/mm	a/mm
1	-	0.3	1
2	-0.3	-	0.8
3	-0.1	-0.8	0.5
4	-	-0.1	-1
5	-	-0.3	-0.3
6	-	1	1

The steps of the distance constraint simulation identification experiment are the same as the above-mentioned angle parameter-based simulation identification experiment and will not be repeated here. The identification results are shown in Table 5.

Table 5. The identified joint parameter errors.

Joint i	$\theta/^\circ$	d/mm	a/mm
1	-	0.2850	0.9500
2	-0.3047	-	0.7600
3	-0.1180	-0.7600	0.4750
4	-	-0.0952	-0.7602
5	-	-0.2850	-0.252
6	-	0.9500	0.9500

After all the identified joint parameter errors are compensated into the kinematic model of the tandem robotic arm, the absolute angle accuracy and position accuracy of the tandem robotic arm are verified and a lateral comparison with methods based only on distance constraints is produced. The results are shown in Figure 10. In the position error experiment, a total of 40 simulation experiments were conducted with groups of 10, with each group moving at different distances.

It can be seen from the above results that both the angle accuracy and position accuracy of the robot have been significantly improved after compensation. Before compensation, the maximum value of robot angle error is 0.6832° , the average value is 0.1615° , and the mean square error is 0.1810° ; after compensation, the maximum value of robot angle error is 0.0641° , the average value is 0.0197° , and the mean square error is 0.0172° . Before calibration, the maximum position error of the robot is 1.882 mm, the average position error is 0.4913 mm, and the mean square error is 0.4613 mm; after compensation, the maximum position error of the robot is 0.3800 mm, the average position error is 0.0947 mm, and the mean square error is 0.0960 mm. The position accuracy was improved by 80.7%, and the attitude accuracy was improved by 87.8%.

In this paper, the method of separating and calibrating the error of the angle parameter and the error of the joint length parameter is adopted. It has been experimentally verified that this method can greatly improve the absolute pose accuracy of the robot. To verify the superiority of this method, this method and other comparative experiments of the method further illustrate the advantages of the method.

In this comparative experiment, the calibration method based on distance constraint, the calibration method based on full pose constraint, and the separation calibration method used in this paper are used to calibrate the robot. The calibration set and compensation set used in the experiment are the same. The result obtained is shown in Figure 11. Similarly, in the position error simulation experiment, every 10 times are at the same distance, for a total of 40 times.

From the above results, we can see that, among the three methods, the best angle accuracy of the robot after compensation is the separation calibration method, and the worst is the calibration method based on distance constraints. This is because although all joint parameters of the robot can be calculated based on distance constraints, and because the joint angle parameter error is much smaller than the joint length parameter error, it is easy to be overwhelmed by the length joint error in the identification process, resulting in a large angle parameter identification error, meaning that the robot's angle accuracy is poor. Although the full pose constraint also has this problem, it can slightly improve this problem because it uses the pose constraint. The separation calibration method identifies the joint angle parameter and the joint length parameter separately, so there is no such problem; as such, its pose accuracy is higher. After compensation, the position accuracy of the separation calibration method and the calibration method based on the full pose constraint are almost the same, but both are higher than the position accuracy of the calibration method based on the distance constraint, because the contribution weight of the joint angle parameter

to the end position error is relatively high. Large, high-precision angular parameters also benefit robot position accuracy.

To sum up, the angle accuracy of the separation calibration method is higher than the other two methods, and its position accuracy is also well guaranteed. The separation calibration method is better than the other two methods.

3.2. Tandem Robotic Arm Entity Experiment Results

In the ABB IRB-1200 calibration experiment, after eliminating the measurement data with large error, 65 sets of data are left: 25 sets of attitude measurement data and 40 sets of position measurement data. To reduce the influence of random errors on the calibration results, repeated experiments were carried out several times, and the average value of the measurements was taken. Substitute the obtained pose data into the above-mentioned separation calibration method and obtain the structural parameter error of the serial manipulator as shown in Table 6.

Table 6. The joint parameter errors obtained by identification.

Joint i	$\theta/^\circ$	d/mm	a/mm	$\alpha/^\circ$	$\beta/^\circ$
1	0.0335	0.2975	-0.0772	-0.4661	-
2	0.9675	-	0.0314	0.5465	0.1123
3	-0.2930	-0.0367	0.0174	-0.8628	-
4	-0.2729	0.2377	-0.0865	-0.6019	-
5	0.5736	0.2872	0.0424	0.7824	-
6	-0.5182	0.0936	-0.2615	-0.3927	-

The above results are compensated into the kinematic model of the serial manipulator, and the attitude accuracy and absolute accuracy after compensation are checked. The angle accuracy verification experimental method is shown in Figure 12, and the spatial distance between the camera and the end of the robot is approximately 700 mm. The angle accuracy of the robot is characterized by the difference between the input motion angle and the actual motion angle of the end of the serial manipulator. Randomly select 20 configurations in the joint motion space of the manipulator, and the attitude accuracy of the manipulator after compensation is shown in Figure 13.

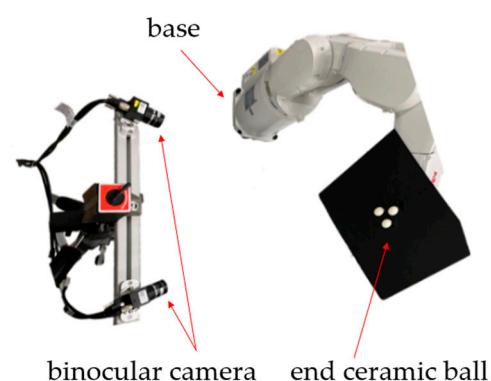


Figure 12. Angle accuracy verification experiment.

It can be seen from Figure 13 that after the IRB-1200 robot is calibrated, its maximum attitude error is reduced from 2.729° to 0.473° , and the average attitude error is reduced from 1.261° before calibration to 0.1735° ; in addition, the mean square error is reduced from 0.7300° to 0.0923° , and the absolute attitude accuracy of the robot is significantly improved. The attitude accuracy was improved by 86.2%.

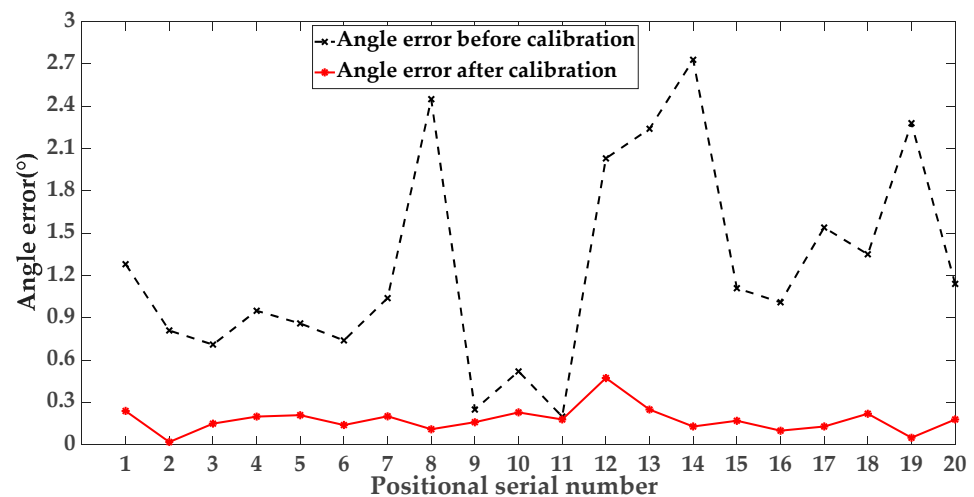


Figure 13. Angle error before and after calibration.

The position error verification experiment is shown in Figure 14; the spatial distance between the camera and the end of the robot is approximately 500–1000 mm. A ceramic standard ball is installed on the calibration board at the end of the robotic arm, and the moving distance of the ball is the moving distance of the robotic arm. The position accuracy of the robotic arm is characterized by the difference between the robot's movement distance and the movement distance measured by the camera.



Figure 14. Position accuracy verification experiment.

In the robot joint motion space, 40 motion distance tests were performed, and the robotic arm was controlled to move four different moving distances of 50 mm, 60 mm, 80 mm, and 100 mm, respectively. The experimental results are shown in Figure 15.

The maximum position error of the IRB-1200 robot is reduced from 1.998 mm to 0.7107 mm after calibration, the average position error is reduced from 0.7873 mm before calibration to 0.2604 mm, and the mean square error is reduced from 0.5262 mm to 0.1272 mm. After calibration, the absolute position accuracy of the robot is significantly improved. The position accuracy was improved by 66.9%.

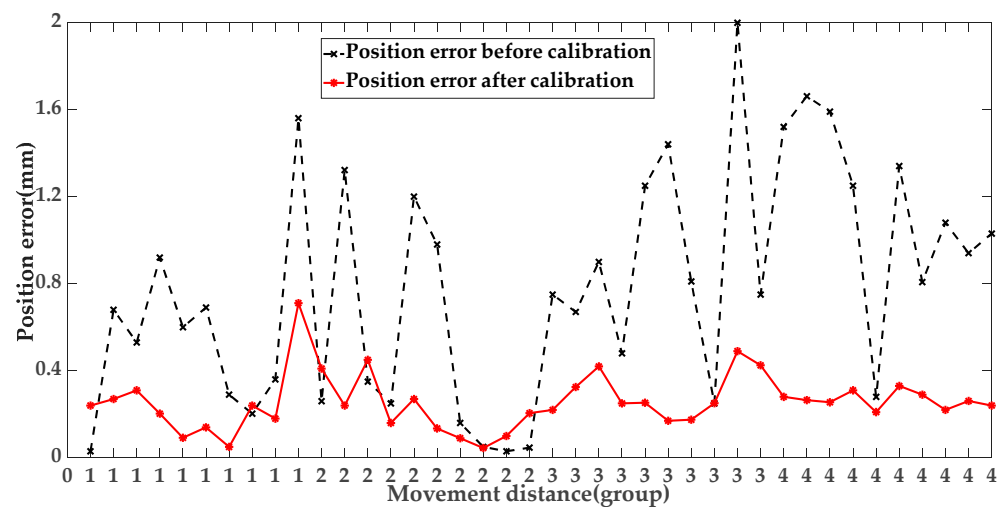


Figure 15. Position error before and after calibration.

4. Conclusions

This paper proposes a method for separating and calibrating structural parameters of 6R series manipulators based on binocular vision. As a tool for end pose measurement, the binocular camera improves the automation level in the measurement process and greatly improves the calibration efficiency. The angle joint parameters and the length joint parameters are separated and calibrated, which avoids the problem that the angle joint parameters are submerged by the length joint parameter errors in the parameter identification process. The joint parameter error identification distance constraint is completed through the angle constraints and angle constraints, which not only improves the serial robot arm Compared with single distance constraint and full pose constraint parameter identification, but the absolute pose accuracy of the tandem robotic arm is greatly improved. In addition, an ill-conditioned algorithm is used to optimize the identification equation. Like other algorithms, this algorithm has some generality and can be used for other error identification models.

During the research, it was found that during the binocular vision measurement, there was a certain deviation between the contour of the ceramic standard sphere captured by the binocular camera and the actual ceramic standard sphere, which limited the improvement of the calibration accuracy. Therefore, the author will conduct research on the impact of spherical deviation on the accuracy of robotic arms in the future. In addition, geometric error is only a fundamental error that affects the accuracy of the robotic arm, and this problem can be solved through the calibration method proposed in this article. However, there are also factors such as thermal deformation error, gear clearance error, and joint transmission error, which have a significant impact on high-precision important assembly occasions. Therefore, the accuracy of the robotic arm needs to be further improved, and subsequent work will conduct calibration research on the above factors.

Author Contributions: Conceptualization, R.W.; Software, X.G. and S.L.; Formal analysis, R.W. and X.G.; Resources, L.W.; Writing—original draft, X.G.; Writing—review & editing, X.G. and S.L.; Visualization, R.W.; Funding acquisition, R.W. and L.W. All authors have read and agreed to the published version of the manuscript.

Funding: This research was funded by National Natural Science Foundation of China (Grant No. 51975157).

Data Availability Statement: Not applicable.

Acknowledgments: The authors are thankful to reviewers and the editor for their valuable suggestions and comments which improve the manuscript a lot.

Conflicts of Interest: The authors declare no conflict of interest.

References

1. Joubair, A.; Bonev, I.A. Kinematic calibration of a six-axis serial robot using distance and sphere constraints. *Int. J. Adv. Manuf. Technol.* **2015**, *77*, 515–523. [[CrossRef](#)]
2. Ding, X.; Zhou, L.; Zhou, J. Pose error analysis of robot in three dimension. *J. Beijing Univ. Aeronaut. Astronaut.* **2009**, *35*, 241–245.
3. Nubiola, A.; Bonev, I.A. Absolute calibration of an ABB IRB 1600 robot using a laser tracker. *Robot. Comput.-Integr. Manuf.* **2013**, *29*, 236–245. [[CrossRef](#)]
4. Gao, G.; Sun, G.; Na, J. Structural Parameter Identification for 6 Dof Industrial Robots. *Mech. Syst. Signal. Pr.* **2018**, *113*, 145–155. [[CrossRef](#)]
5. Schröer, K.; Albright, S.L.; Grethlein, M. Complete, Minimal and model-continuous kinematic models for robot calibration. *Robot. Cim.-Int. Manuf.* **1997**, *13*, 73–85. [[CrossRef](#)]
6. Samad, A.H.; Hayati, S. Robot arm geometric link parameter estimation. In Proceedings of the IEEE Conference on Decision & Control, San Antonio, TX, USA, 14–16 December 1983.
7. Veitschegger, W.; Wu, C.H. A method for calibration and compensation of robot kinematic errors. In Proceedings of the IEEE ICRA, Raleigh, NC, USA, 31 March–3 April 1987.
8. Stone, H.W.; Sanderson, A.C. Statistical performance evaluation of the S-model arm signature identification technique. In Proceedings of the IEEE ICRA, Philadelphia, PA, USA, 24–29 April 1988.
9. Zhuang, H.; Roth, Z.S.; Hamano, F. A complete and parametrically continuous kinematic model for robot manipulators. In Proceedings of the IEEE ICRA, Cincinnati, OH, USA, 13–18 May 1990.
10. Lv, L.; Li, X.H.; Fei, S.X. Kinematics Modeling and Analysis of 6R Manipulator Based on Screw Method. *J. Chifeng Univ.* **2019**, *35*, 53–55.
11. Chen, I.; Yang, G.; Tan, C.T. Local Poe Model for Robot Kinematic Calibration. *Mech. Mach. Theory* **2001**, *36*, 1215–1239. [[CrossRef](#)]
12. Yin, J.; Gao, Y. Pose Accuracy Calibration of a Serial Five DOF Robot. *Energy Procedia* **2012**, *14*, 977–982. [[CrossRef](#)]
13. Xie, Z.; Zong, P.; Yao, P.; Ren, P. Calibration of 6-DOF industrial robots based on line structured light. *Optik* **2019**, *183*, 1166–1178. [[CrossRef](#)]
14. Wang, F. Research on the monitoring method of robotic arm end pose based on image visual features. *Mach. Des. Manuf.* **2023**, 1–5. (In Chinese)
15. Yang, J.; Wang, D.; Fan, B.; Dong, D.; Zhou, W. Online Absolute Pose Compensation and Steering Control of Industrial Robot Based on Six Degrees of Freedom Laser Measurement. *Opt. Eng.* **2017**, *56*, 34111. [[CrossRef](#)]
16. Lgnani, G.; Tiboni, M. Optimal design and application of a low-cost wire-sensor system for the kinematic calibration of industrial manipulators. *Mech. Mach. Theory* **2014**, *73*, 25–48. [[CrossRef](#)]
17. Olarra, A.; Axinte, D.; Kortaberria, G. Geometrical calibration and uncertainty estimation methodology for a novel self-propelled miniature robotic machine tool. *Robot. Cim.-Int. Manuf.* **2018**, *49*, 204–214. [[CrossRef](#)]
18. Jiang, Z.X.; Qin, P.J.; Su, R. High precision visual monitoring of robotic arm pose based on deep learning. *Modul. Mach. Tools Autom. Manuf. Tech.* **2022**, *11*, 138–142.
19. Lu, Y.; Shen, T.X.; Luo, Z. Calibration of kinematics parameters of industrial robot based on linear structured light Sensor. *Acta Metrol. Sin.* **2021**, *42*, 66–71.
20. Luo, Z.J.; Sun, S.J.; Mei, J.P. Research on robot calibration application based on wire displacement sensor. *Aeronaut. Manuf. Technol.* **2017**, *9*, 43–49.
21. Balanji, H.M.; Turgut, A.E.; Tunc, L.T. A novel vision-based calibration framework for industrial robotic manipulators. *Robot. Cim.-Int. Manuf.* **2022**, *73*, 102248. [[CrossRef](#)]
22. Rozlivek, J.; Rustler, L.; Stepanova, K. Multisensorial robot calibration framework and toolbox. In Proceedings of the IEEE-RAS, Munich, Germany, 15–17 November 2021.
23. Li, Z.B.; Li, S.; Luo, X. Using Quadratic Interpolated Beetle Antennae Search to Enhance Robot Arm Calibration Accuracy. In Proceedings of the IEEE-RAL, Xishuangbanna, China, 5–9 December 2022.
24. Wang, X.L.; An, L.X.; Zhang, H.Z. Error analysis and simulation research of manipulator based on calibration method of kinematics parameters. *Mech. Electr. Eng.* **2019**, *36*, 109–116.
25. Urrea, C.; Pascal, J. Design, simulation, comparison and evaluation of parameter identification methods for an industrial robot. *Comput. Electr. Eng.* **2018**, *67*, 791–806. [[CrossRef](#)]
26. Chen, X.; Zhang, Q.; Sun, Y. Non-kinematic Calibration of Industrial Robots Using a Rigid-flexible Coupling Error Model and a Full Pose Measurement Method. *Robot. Cim.-Int. Manuf.* **2019**, *57*, 46–58. [[CrossRef](#)]
27. Dolinsky, J.U.; Jenkinson, I.D.; Colquhoun, G.J. Application of Genetic Programming to the Calibration of Industrial Robots. *Comput. Ind.* **2007**, *58*, 255–264. [[CrossRef](#)]
28. Lattanzi, L.; Cristalli, C.; Massa, D. Geometrical calibration of a 6-axis robotic arm for high accuracy manufacturing task. *Int. J. Adv. Manuf. Technol.* **2020**, *111*, 1813–1829. [[CrossRef](#)]
29. Shi, Y.Q.; Li, K.F.; Lu, R.S. Kinematics parameter identification of industrial robot based on binocular vision. *Laser Optoelectron. Prog.* **2022**, 1–13. (In Chinese)
30. Xing, Y.L.; Li, L. A method for calibration of mechanical arm structural parameters based on exponential product. *Manuf. Autom.* **2023**, *45*, 12–45.

31. Grotjahn, M.; Daemi, M.; Heimann, B. Friction and rigid body identification of robot dynamics. *Int. J. Solids Struct.* **2001**, *38*, 1889–1902. [[CrossRef](#)]
32. Zhao, Z.Y. *Research on Generalized Kinematics Error Calibration Method of Serial Industrial Robot*; Harbin Institute of Technology: Harbin, China, 2022.
33. Chen, X. *Research on Closed-Loop Calibration Method for 6R Robot Based on Machine Vision*; Harbin Institute of Technology: Harbin, China, 2019.
34. Nguyen, H.N.; Le, P.N.; Kang, H.J. A new calibration method for enhancing robot position accuracy by combining a robot model-based identification approach and an artificial neural network-based error compensation technique. *AIME* **2019**, *11*, 168781401882293. [[CrossRef](#)]
35. Yan, Y. Error recognition of robot kinematics parameters based on genetic algorithms. *JAIHC* **2020**, *11*, 6167–6176. [[CrossRef](#)]
36. Kosmatopoulos, E.B.; Chassiakos, A.; Christodoulou, M.A. Robot Identification using Dynamical Neural Networks. *Eng. Syst. Intell.* **1992**, *9*, 187–195.
37. Peng, G.L. *Research on Kinematics Calibration Method of XYZ-3RPS Six Axis Hybrid Machining Equipment*; Harbin Institute of Technology: Harbin, China, 2021.

Disclaimer/Publisher’s Note: The statements, opinions and data contained in all publications are solely those of the individual author(s) and contributor(s) and not of MDPI and/or the editor(s). MDPI and/or the editor(s) disclaim responsibility for any injury to people or property resulting from any ideas, methods, instructions or products referred to in the content.